LPBF Fabrication of Thin Cross Sections: Challenges and Printability

John Daniel Arputharaj, Shahrooz Nafisi, and Reza Ghomashchi

Abstract Additive Manufacturing (AM) as a prototyping technique has recently evolved into a stand-alone manufacturing process. Laser Powder Bed Fusion (LPBF), also known as Selective Laser Melting (SLM), as the most commonly used technique for metal additive manufacturing uses a laser as the energy source to melt and shape complex designs. The increased freedom in design has offered a shorter assembly line, lower parts weight, shorter lead time, and efficient materials usage. However, the high demand in the aerospace, medical, and automotive industries for even lighter artifacts has opened a new field for designing and fabricating lattice-architectured metamaterials. These miniature networked designs have been mainly researched to establish the variation in the macro-mechanical properties while ignoring the strut's topological integrity and microstructure, all controlled by the process parameters. To have a clearer understanding of the topological and microstructural evolution in thin sections, this work aims at studying the geometrical and microstructural features of single struts of varying diameters ranging from 0.1 to 1 mm within the XY plane and angles from 10° to 90° in the z-direction to establish the capability of LPBF machines in printing struts as the essential constituent of the lattice structures. In this regard, the printability of struts with respect to their diameter, length, angle of inclination, circularity, and surface integrity are studied and discussed. The analysis of the results suggests that to successfully manufacture a lattice structure, struts as the main constituent of lattice architecture should have any diameter above 0.2 mm with an angle of inclination between 40° and 60° to exhibit good geometrical accuracy, lower surface roughness, and lower hardness.

Keywords Additive manufacturing · LPBF · Strut · Ti6Al4V · Solidification · Print angle · Circularity

J. D. Arputharaj (✉) · S. Nafisi · R. Ghomashchi
School of Mechanical Engineering, University of Adelaide, Adelaide, SA 5000, Australia
e-mail: john.arputharaj@adelaide.edu.au

The Minerals, Metals & Materials Society, *TMS 2023 152nd Annual Meeting & Exhibition Supplemental Proceedings*, The Minerals, Metals & Materials Series,
https://doi.org/10.1007/978-3-031-22524-6_16

Introduction

Fabrication of precise and fine detailed components with a higher definition for engineering [1, 2] and biomedical [3, 4] applications has helped Laser Powder Bed Fusion (LPBF) to evolve as one of the prospectus Additive Manufacturing (AM) techniques of the present and the future. Lattice structures are the most recent fascination of the metal additive manufacturing industry as it enables the fabrication of metallic structures with reduced weight, hence bringing in a host of improved mechanical properties such as lower Young's modulus [5–8] and the ability to absorb more energy on impact [5, 9–12]. The lattice architecture is principally based on the introduction of printing of topologically intertwined struts. The integrity of the lattice structure is mainly based on the quality of struts. Therefore, knowledge of printing struts of better quality is paramount to fabricating high-quality lattice structures. Studies have previously been done to establish the manufacturability of single struts in LPBF and EBM to estimate the manufacturable ranges for the successful fabrication of lattices [13–15]. Several difficulties were encountered with respect to the fabrication of the lattice structures such as the inconsistency with the minimum manufacturable diameter for machines of different manufacturers, internal defects, and deviation from the design parameters have been reported [13–16]. The morphology and cause of these defects such as porosity and the percentage deviation from the design concerning geometric parameters haven't been established sufficiently. The reported works fabricated single struts aligned with either the X- or Y-axis with an angle increasing in the Z direction. But in real-life manufacturing of lattice structures, most of these struts will be inclined at inclination angles between 30° and 60° in both X and Y directions with varying angles on the Z-axis [9, 17–20]. The current study reports on attempts to fabricate single struts on the XY plane with increments of the inclination angle along the Z-axis to analyze the geometrical accuracy, bulk, and surface integrity and their effects on the mechanical robustness, and hardness of these struts.

Experimental Procedures

Materials and LPBF Equipment

The strut samples used in this study were made of Ti6Al4V (Ti64) fabricated using the LPBF technique. This study aims at studying the printability of continuous laser deposition of Ti6Al4V 10 mm long fine cylinders of various diameters and angles of inclination. This study was undertaken with the motivation to identify the manufacturing limit for struts of high mechanical integrity. The gas atomized pre-alloyed Ti64 alloy powder was supplied by TLS, Technik GmbH & Co [21]. The alloy powder composition was analyzed, and its size distribution was checked using a range of analytical techniques. Inductively coupled Plasma Atomic Emission Spectroscopy (ICP-AES) was used to analyze the chemical composition of the metallic elements

such as Al, Ti, Fe, and V. A LECO ONH836 elemental analyzer was used to measure the gaseous impurities (oxygen, nitrogen, and hydrogen) while the carbon impurity percentage, was measured on a LECO CS200, the carbon, and sulfur analyzer for metals. The chemical composition of the Ti6Al4V powder is given in Table 1. The main alloying elements, Ti, Al, and V, and the level of impurities are in the acceptable range as per the ASTM F2924-14 [22], also given in Table 1. A laser particle size analyzer, Mastersizer 2000, was used to verify the powder size distribution characteristics and confirmed the median size of the powder being 22.75 μm. The powder particle morphology was also analyzed in a FEG-SEM (FEI Quanta 450) confirming spherical morphology which is typical of the gas atomization process for powder production. Figure 1 shows an SEM micrograph of the spherical morphology of the powder particles along with the powder size distribution [23].

The strut samples were manufactured using a 3D systems Pro-X 200 DMP having a laser with a maximum power of 300 W that irradiates the powder in a continuous mode with a wavelength of 1070 nm and Focal Offset Distance (FOD) of 2 mm giving rise to 70 μm probe size. The manufacturing chamber is maintained in a high-purity argon atmosphere of 101 kPa to ensure that the oxygen level is lesser than 500 ppm throughout the process. The process parameters used in this study (Table 2) have been previously established in a study focused on manufacturing parts of the highest relative density (99.86%) [23]. The samples were designed using Autodesk NetFabb 2022 and Autodesk Fusion 360. The scan strategy for these struts

Table 1 Chemical composition of Ti6Al4V powder and ASTM F2924-14 standard composition (wt%) [22]

Item	V	Al	Fe	O	C	N	H	Ti
Powder	3.94	6.15	0.18	0.098	0.005	0.010	<0.002	Bal
ASTM F2924-14	3.50–4.50	5.50–6.75	Max 0.3	Max 0.2	Max 0.08	Max 0.05	Max 0.015	Bal

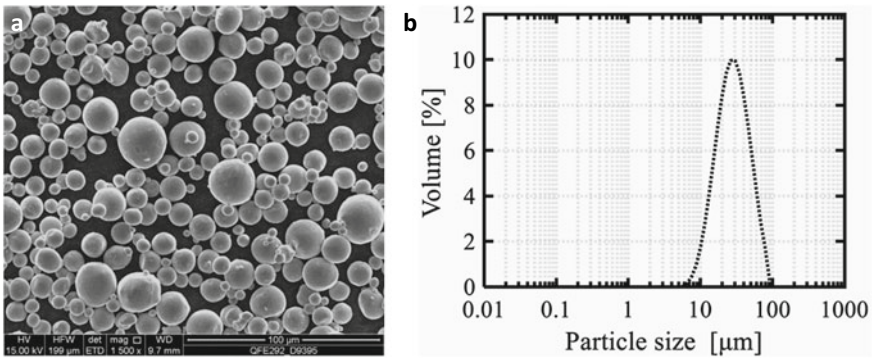

Fig. 1 **a** SEM image showing the typical as-received Ti64 powder (scale bar 100 μm) and **b** powder size distribution [23]

Table 2 Continuous mode of LPBF—process parameters

Laser power, P (W)	Hatch space, h (μm)	Scanning velocity, v (mm/s)	Layer thickness, t (μm)	Beam spot size, w_0 (μm)	Focal offset distance (FOD) (mm)
270	85	1800	30	70	2

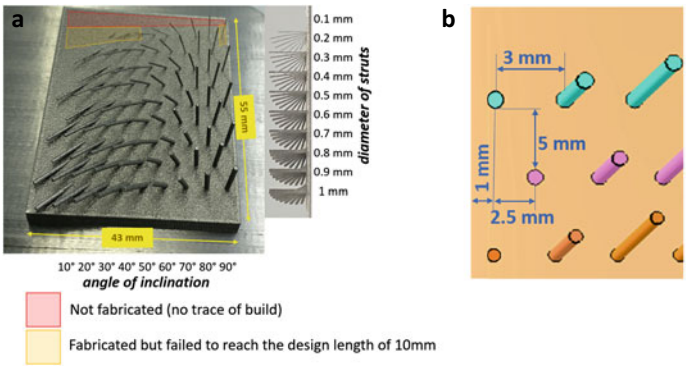

Fig. 2 **a** Strut plate's design, **b** Struts locations on the plate

is a bidirectional strategy with an interlayer 90° rotation, commonly known as the "crisscross" pattern. The designed single struts range from a diameter of 0.1–1 mm with varying inclination angles of 10°–90°, as illustrated in Fig. 2.

The angle of inclination was kept constant at 45° with respect to both X and Y directions and varied along the Z-axis from 10° to 90° with increments of 10°. This design strategy was chosen to understand the manufacturability of the struts concerning geometrical parameters implemented in most of the lattice configurations. To have the most compact arrangement and to avoid the overlap of the struts, certain precautions such as offsetting the arrangement of the struts, depicted in Fig. 2b, were taken. To reduce the likelihood of damaging the Ti (CP) base plate and the printed struts during removal, a plate with 3 mm thickness was initially printed as the base plate for struts (strut plate). The fabricated strut plate is viewed in Fig. 2a.

Analysis Techniques

The geometrical and microstructural analyses carried out in this study intended at evaluating the ability of the continuous mode of LPBF 3D printing technology in fabricating struts, the main structural component of lattice architecture. Initial visual and stereoscope inspections were to identify the struts that failed to manufacture due to the extremities of the angle of inclination and/or the diameter. Then, the struts were removed from the strut plate using a diamond cutting wheel (diameter 20 mm) at 1000

RPM, and their surface profile (roughness) was measured using an Olympus LEXT OLS5000 laser profilometer with an incident laser beam wavelength of 405 nm. The samples were mounted for metallographic investigation by vacuum impregnation of epoxy resin into the mount. The samples were made to stand straight irrespective of the deposited angle of inclination to ensure that all the surfaces viewed are a perfect transverse section.

The samples were ground and polished using the Struers Tegramin-25 and examined by Zeiss Axio Imager optical microscope and FEI Quanta 450 FEG-SEM. The unetched samples were used to measure the circularity and porosity content of the deposited struts. Image J software[1] was used to calculate the circularity and measure porosity content. Circularity (f_2) is the ratio of the cross-sectional area (A) of the struts to the perimeter (L) of the struts, Eq. 1 [24].

$$f_2 = \frac{4\pi A}{L^2} \tag{1}$$

The hardness of the mounted samples was measured using a Vickers microhardness tester, LECO LM-700AT, with a 50g load and a dwell time of 10s. A total of five indentations per sample were performed at different locations of each strut. The samples were then etched using Kroll's reagent (3% HF + 5% HNO_3 + 92% distilled water) for 35 s for metallographic investigation.

Results and Discussion

Manufacturability

The individual struts were analyzed to determine the manufacturability and mechanical integrity. The struts were manufactured with layers deposition having a crisscross strategy at a fixed direction of ±45° in the X and Y plane with varying angles of inclination along the build direction axis Z from +10° to +90°. To measure the manufacturability, a matrix was made based upon the manufactured strut's length, diameter, and angle of inclination, respectively. As illustrated in the matrix, Fig. 3, 83% of the struts were successfully manufactured to the entire length except for the low-diameter struts with the extremities of the angles. The 0.1 mm diameter struts were not seen on the strut plate as the small diameter of 0.1 mm renders a small contact surface area of the strut with the strut plate which has resulted in failing to establish a strong bond with the strut plate. In addition, the contact angle between the Ti6Al4V strut plate and the deposited Ti6Al4V strut is around ≈85.2° [25], which means despite partial wetting, the high wetting angle may have resulted in weak bonding. Therefore, the 0.1 mm struts did not appear on the strut plate. In addition,

[1] **ImageJ** is a Java-based image processing program developed at the National Institutes of Health and LOCI, University of Wisconsin.

there are other struts angles and diameters which failed to be printed in accordance with the design criteria as illustrated by the chart in Fig. 3, (yellow region). The 10°, 20°, and 90° inclination angles for 0.2 mm diameter struts were not manufactured to the designed length of 10 mm. The strut of 90° inclination for the 0.2 mm strut must have failed to complete the entire length due to the movement of the recoater blade over the manufactured product. The struts of 10° and 20° inclination angles were fractured due to the extremities of the angle of inclination as the heating zone has more overhang area resulting in high thermal load (the supported zone and the overhang zone are represented in Fig. 4a, b).

As the angle of inclination decreases, the successive layer does not cover the entire surface area of the previous layer which means the steps formed have greater tread as schematically shown in Fig. 4. The depth of the step tread is calculated from the equation below obtained from the geometrical analysis shown on the schematic diagram in Fig. 4.

$$\tan(90 - \theta) = \frac{\text{Step tread}}{\text{Step rise}}$$

where the step rise is the powder layer thickness (30 μm) and the step tread is the length hanging over for each layer, (overhang depth). For example, the step tread for 10° inclination is ~170 μm which is hanging over the previous layer. This means the contact area between consecutive layers is small, i.e. bond strength between the layers is reduced. As the printing length increases, the gravitational forces may exceed the bond strength of the two consecutive layers and the strength of the strut itself, knowing that the temperature increases during printing and thus the strength of the alloy decreases. In addition, the lack of complete overlapping of consecutive layers may result in slight changes in the cooling rate of each deposited layer at a

Diameter (mm) \ Angle of inclination in Z axis		10°	20°	30°	40°	50°	60°	70°	80°	90°
0.1	Fabricated length (mm)	0	0	0	0	0	0	0	0	0
	Fabricated angle in Z axis (°)	0	0	0	0	0	0	0	0	0
0.2	Fabricated length (mm)	3	5.5	10	10	10	10	10	10	8.2
	Fabricated angle in Z axis (°)	12.5	20.5	26.5	35.5	46	54	62	71	88
0.3	Fabricated length (mm)	10	10	10	10	10	10	10	10	10
	Fabricated angle in Z axis (°)	12.5	20	37	43	48	59	69	75	89
0.4	Fabricated length (mm)	10	10	10	10	10	10	10	10	10
	Fabricated angle in Z axis (°)	11.5	16	31.5	41.5	46	60	70	74	86
0.5	Fabricated length (mm)	10	10	10	10	10	10	10	10	10
	Fabricated angle in Z axis (°)	7.5	13.5	38	47	48.5	57	69	80	90

Diameter (mm) \ Angle of inclination in Z axis		10°	20°	30°	40°	50°	60°	70°	80°	90°
0.6	Fabricated length (mm)	10	10	10	10	10	10	10	10	10
	Fabricated angle in Z axis (°)	6.5	13.5	31.5	44.5	48.5	57	69	80	90
0.7	Fabricated length (mm)	10	10	10	10	10	10	10	10	10
	Fabricated angle in Z axis (°)	6.5	18	32.5	42.5	50	60	70	80	90
0.8	Fabricated length (mm)	10	10	10	10	10	10	10	10	10
	Fabricated angle in Z axis (°)	7	20	32.5	40	50	60	70	80	90
0.9	Fabricated length (mm)	10	10	10	10	10	10	10	10	10
	Fabricated angle in Z axis (°)	6.5	19	32.5	40	50	60	70	80	90
1.0	Fabricated length (mm)	10	10	10	10	10	10	10	10	10
	Fabricated angle in Z axis (°)	5	16	30	40	50	60	70	80	90

Not Fabricated (no trace of build)

Fabricated but failed before reaching the design length/angle of inclination

Successfully manufactured to designed length and angle of inclination

Fig. 3 Manufacturability of struts of different diameters and varying angles along the build direction Z

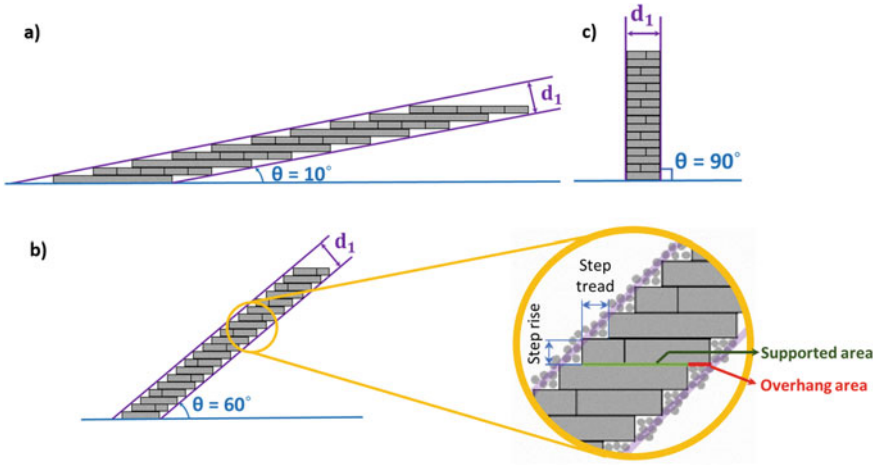

Fig. 4 The stepwise nature of strut deposition at different angles of inclinations; **a** 10° **b** 60° **c** 90°

time. This may result in the formation of a wider residual stress distribution during cooling to provide more distortion. With a higher angle of inclination, between 60° and 90°, there is hardly any deviation from the designed angle of inclination as every layer is deposited over the previous layer resulting in smaller step tread, for example, for an inclination angle of 60, the step tread is ~50 μm in contrast to 170 μm for 10° inclination angle, results in better compliance with the designed inclination angle.

Dimensional Accuracy

When printing the lattice structures, the struts come in a range of angles from 90° inclination to around 30° depending on the topology of the designed lattice sub-structural unit, e.g. BCC, FCC, etc. [17, 26]. The changes in angle impart some changes in the shape of struts that were designed as cylinders. To confirm the ability of 3D printing of struts at different angles of inclination, it is required to examine their circularity. A perfect cylinder has a circular cross-section with a circularity of 1. Circularity measurements were taken on the cross-section (transverse) of the struts after removing them from the strut plate and sectioning them as depicted in Fig. 5, to establish the ability of the ProX200 printer in printing cylindrical struts with the originally designed dimension.

Figure 6 is an example of the struts of 0.9 and 0.5 mm diameters with a range of inclination angles that were mounted in a vertical position as represented in the schematic diagram in Fig. 5, and their transverse sections' circularity was analyzed. The uneven morphology of the top surface of struts can influence the measurements and hence the struts were mounted upright irrespective of their angle of inclination, and polished to view the transverse section as represented in Fig. 6. For vertically

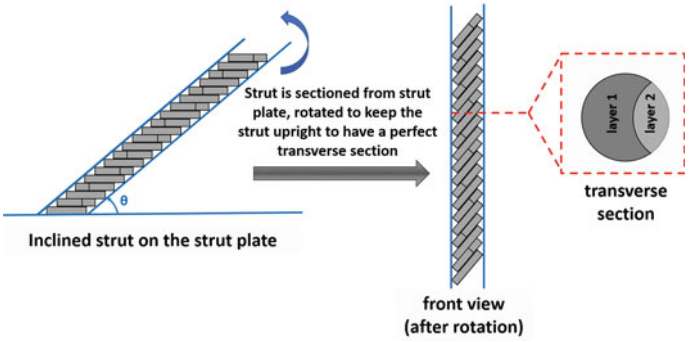

Fig. 5 Schematic of the layer arrangement and the transverse sectioning for metallography

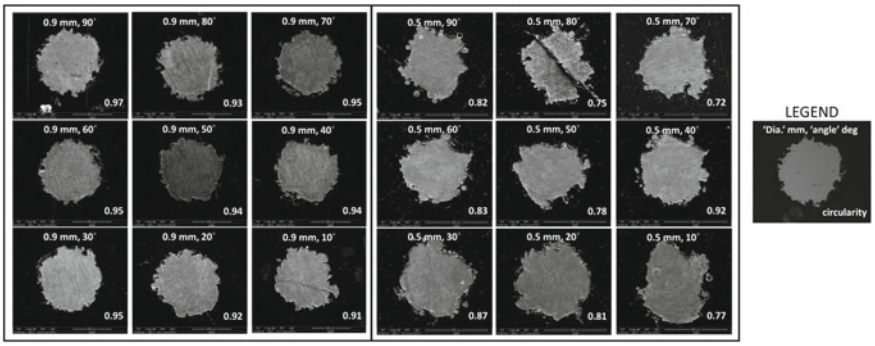

Fig. 6 Transverse view of 0.9 mm (scale bar 500 μm), and 0.5 mm struts (scale bar 400 μm), of various angles of inclination

built struts (inclination angle of 90°), it was found that the circularity is around 0.97 (closer to the circularity of a circle, 1) for 0.9 mm diameter and closer to 0.8 for 0.5 mm diameter struts. This signifies that as the diameter is decreasing, the circularity decreases. The shift in circularity is due to the increase in the offset of the melt pool as the angle of inclination decreases. In addition to the offsetting of the melt pool, the lower angle of inclination results in the flow of the molten liquid in the direction of gravity.

Porosity and Roughness

During the printing process, the width of the melt pool has to be overlapping the previous track and partially overlap the lateral adjacent track (hatch space) to ensure high density and sound metallurgical bonding [27, 28]. The sound bonding between the layers and lateral scan track can prevent the evolution of porosity due to the

lack of fusion in the bulk of the LPBF samples [29–31]. In addition to inter-track porosity, the surface topography of the prior layer can influence the probability of porosity formation, meaning that whether the melt pool of the following track is able to fully wet the prior track [32, 33]. Furthermore, in the case of the inclined struts, the gravitational force makes the molten pool flow downwards around the over-hanging step tread (Fig. 4a) which solidifies rapidly due to the high cooling rate of the LPBF process [26, 34]. This may result in forming an irregular profile around the periphery of struts containing porosity of varying morphology. Since such porosity arises due to the flow overlay of the molten pool over a solidified region, it may be identified as flow line gaps, Fig. 7a. The flow line gaps are mostly seen near the lower surface of the inclined struts and the aspect ratio (length/width) of the porosity is around ~10. The frequency of the elongated porosity reduces with increasing inclination angles and larger diameter struts as there is less flow of melt pool over the sides. In addition to the above-mentioned geometry and process-controlled porosity, the entrapment of gases generated due to partial evaporation during powder bed irradiation or the inert gas of the printing chamber results in the formation of gas porosity. The gas porosity was mainly detected in the struts with a higher inclination angle (70°–90°). They contain small spherical pores of a diameter of 3 ± 1 μm in the center of the struts, which arises due to the entrapment of gases during the rapid solidification, Fig. 7b. For the lower angle of inclination struts, most of the porosity content is seen around the strut periphery with elongated morphology as the molten metal tends to flow to the side within the melt pool lifetime due to the gravitational forces.

The surface roughness of struts is also affected by the topological and geometrical parameters of the angle of inclination and the actual diameter, respectively. It can be inferred from Fig. 8 that as the angle of inclination decreases, the melt pool flow lines become more distinct. The detection of the actual layer flow line confirms the lack of overlapping/supporting of consecutive layers and the formation of more distinct over-hanging steps with reduction in inclination angle. The severity of over-hanging

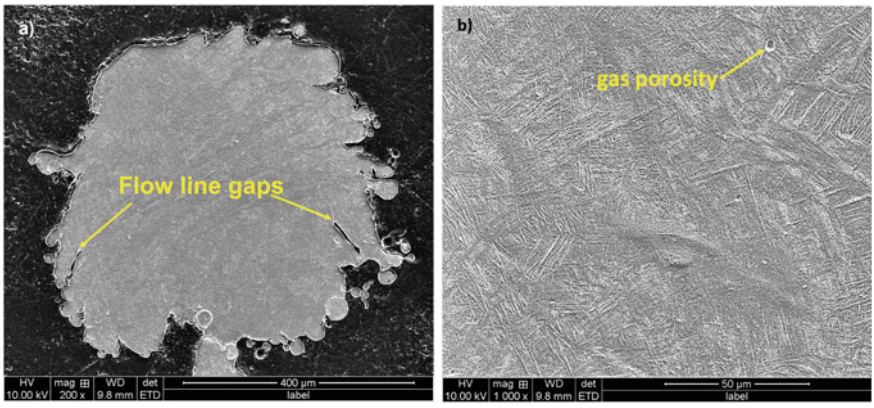

Fig. 7 **a** Peripheral flow line gaps **b** spherical gas porosity (0.7 mm dia. strut at 10° inclination)

steps increases with decreasing strut diameter if the 1 and 0.2 mm diameter struts are compared, Fig. 8. These are the main reasons for increasing the instability of struts and their premature failure before reaching the full designed length. The effect on roughness however appears to be the reverse where by reducing the diameter, the instability of over-hanging steps is more pronounced as the bond area between the layers is smaller. This has caused the solidified molten pool to bend over the prior layer reducing the roughness physically as schematically shown in Fig. 9. The over-hanging step for the d_1 diameter strut is more prone to bend over the layer below than the d_2 diameter strut as the contact area between consecutive layers is smaller for the smaller diameter strut. The susceptibility of over-hanging steps to bend over the prior layer is greater with decreasing struts diameter. Moreover, as the angle of inclination increases the surface topography approaches those of sintered powder, i.e. spongy appearance with distinct sintered satellite particles, Fig. 9.

To establish the roughness of the struts quantitatively, the mean roughness depth (Rz) that provides a measure of the average between the highest peaks and the lowest valleys is considered [35]. The Rz helps to identify the effect of the overhangs due to inclination angle over the roughness of the struts. As the inclination angle increases, the detection of flow lines becomes more difficult as the degree of overlapping of consecutive layers increases and the severity of over-hanging steps reduces (hence a reduction in Rz). This results in the surface topography of the struts being more uniform, and both the roughness parameters reduce as shown in Fig. 10. Figure 10 shows that there is an optimum inclination angle of 40°–60° where the lowest roughness value is achieved regardless of strut diameter, the roughness parameter Rz for 90° is the lowest irrespective of the strut diameter as there are no overhang structures,

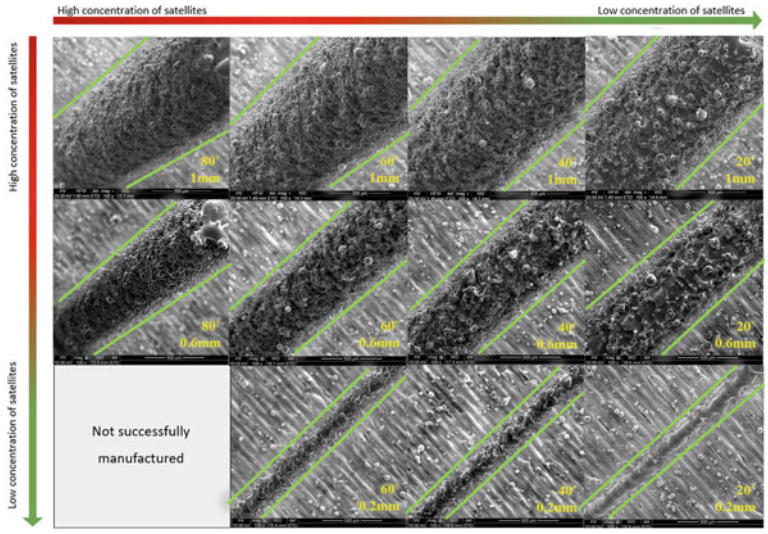

Fig. 8 Formation of melt flow lines and spongy appearance of the surface with angle of inclination for all diameters (scale bar is 500 μm)

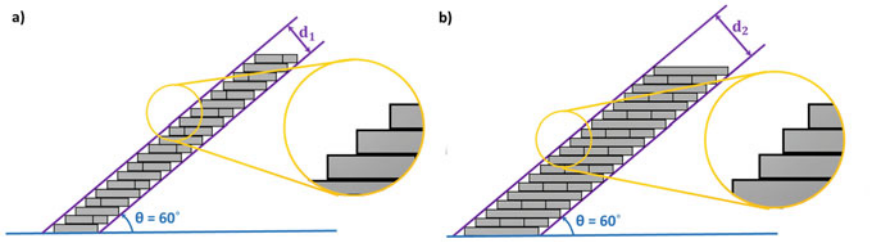

Fig. 9 Schematic diagram showing the bond area between consecutive layers for different diameters ($d_1 < d_2$) struts

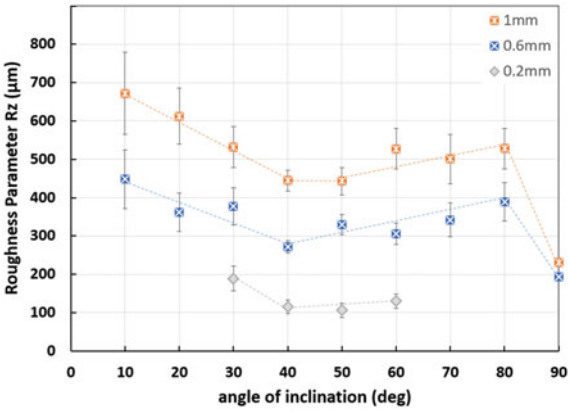

Fig. 10 Rz of 1.0, 0.6 and 0.2 mm struts

Fig. 4c. This is probably due to the combined effect of reduction in over-hanging step and still bending over the previous layer. The fact that struts with larger diameters showed greater roughness value may be attributed to a greater number of tracks and layers where each layer may somewhat magnify the topography of the previous layer related to the ability of the melt pool to wet the already deposited layer.

Microstructural Characterization

The vertical (90° inclination angle) struts have the lowest hardness of 385 ± 12 HV which may be attributed to the thicker diameter (0.9 mm), the zero offset, and perfect layer-over-layer deposition that resulted in sufficient reheating of the prior layer by the deposition of the following layer imposing some degree of stress relieving generated due to rapid solidification of melt pool as it is the characteristics of the LPBF process. However, as the angle of inclination decreases, the heating zone moves, and thus certain parts of prior layers may not receive the same level of

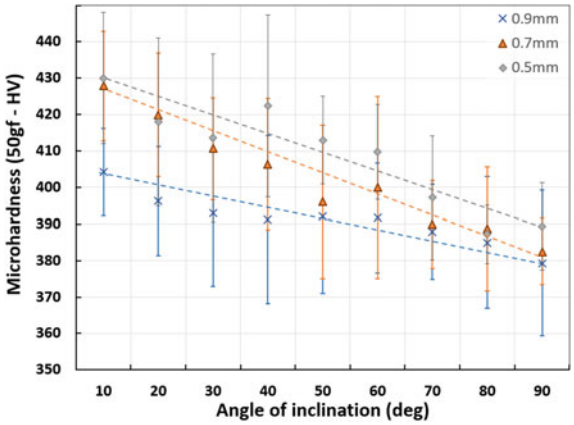

Fig. 11 Microhardness values

reheating, and thus less relieving of the stresses may result. A similar trend is noticed with the decrease in the diameter of the strut as depicted in Fig. 11.

The microstructural analysis reveals the formation of α′ martensite needles as expected due to rapid cooling characteristics of LPBF, Fig. 12. As the inclination angle decreases, there is a weak refinement in the microstructure which may be due to the movement of the heat zone where part of the lower layers does not receive the thermal energy due to the deposition of the following layers. The diameter of the strut appears to be a less definitive factor in altering the microstructure scale as there is hardly any distinction in martensitic lath size for 0.9, 0.6, and 0.3-mm strut diameters, absence of a more distinct change in microstructure scale with strut diameter, may suggest that the cooling rates/the effect of reheating of successive layers are almost the same as the sizes are not that much different. Furthermore, there is a strut plate printed prior to strut printing which means the temperature rise for printing the strut plate may possibly have dampened the effect of strut diameter on cooling rate, i.e. acting as a preheat. The effect of diameter and inclination angle of struts may be better recognized if the microhardness values (Fig. 11) for the three representative strut diameters of 0.9, 0.6, and 0.3 mm are compared. Moreover, the higher hardness could be due to the slight changes in cooling rate experienced by the struts with diameter, although not sufficient to generate a distinct change in microstructure scale, but yet sufficient enough to affect the residual stresses usually experienced during the LPBF process.

Conclusions

The introduction of lattice structure is a new approach in the LPBF manufacturing route to achieve metamaterials with a range of mechanical, physical, and biological properties. They can be tailored for a wide range of applications rendering lighter

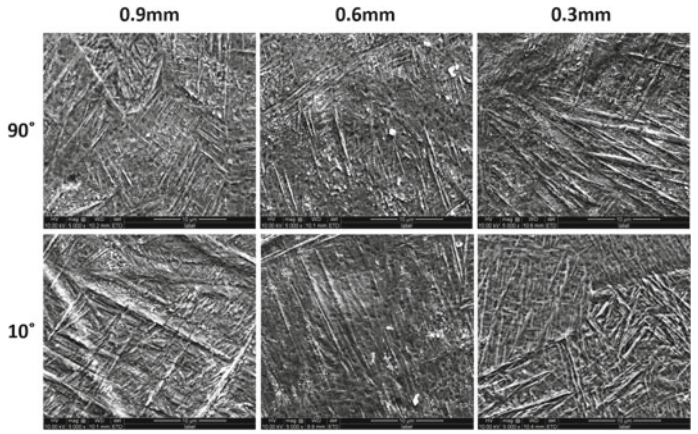

Fig. 12 SEM images of 0.9 mm (scale bar 10 μm), 0.6 mm (scale bar 10 μm), and 0.3 mm (scale bar 10 μm), struts with inclination angles of 90° and10°

yet stronger structures. The success of fabricating these metamaterials is heavily dependent on their structural constituents, the so-called struts. The effect of angle of inclination and diameter of the strut on its geometric, surface, and microstructural characteristics were studied for LPBF of single struts of Ti6Al4V alloy. The quality of the struts achievable through design for the LPBF process can guarantee the integrity of lattice structures. The findings of this study are summarized below.

1. No traces of printing were detected on the strut plate for 0.1 mm diameter struts for the selected optimized process parameters.
2. Some of the struts for the diameter of 0.2 mm could not be manufactured to their designed full length at the extremities of angles, 10°, 20°, and 90° due to changes in thermal and mechanical loading imposed with increasing the printed length. The struts with diameters from 0.3 to 1 mm with different angles of inclination ranging from 10° to 90° were successfully manufactured.
3. The roughness of the struts can be attributed to two aspects of the presence of sintered particles and the flow lines of the melt pool. The former is responsible for the roughness of the surface of a higher angle of inclination strut and the latter for a lower angle of inclination.
4. The main defects were gas porosities and flow line gaps. They occur in two different morphologies of spherical gas porosity, generally occurs in the bulk of the struts and the elongated flow line gaps along the periphery due to melt pool overlay over the previously solidified layers.
5. The inclination angle should always be above 30° to ensure that the manufactured struts are of good geometric accuracy and have fewer overhangs. Overhangs result in undesired surface morphologies such as high roughness and elongated flow line gaps.
6. The hardness of the struts decreases with the increase in the angle of inclination. This may be due to reheating effect of previous layer as layer overlapping

increases with inclination angle, i.e. more efficient localized stress relieving. At lower angles of inclination, the heating zone moves and hence lesser effective reheating.

7. To successfully manufacture a lattice structure, the diameter of struts should be above 0.2 mm with the angle of inclination between 40° and 60° to ensure fabrication of struts with good geometrical accuracy, lower surface roughness, and lower hardness.

Acknowledgements This work was performed in part at the OptoFab node of the Australian National Fabrication Facility (ANFF) utilizing Commonwealth and South Australian State Government funding. Prof. Heike Ebendorff-Heidepriem of IPAS is gratefully acknowledged for access to ANFF facilities. Adelaide Microscopy is gratefully acknowledged for providing access to electron microscopy facilities.

References

1. Banerjee D et al (2013) Acta Mater 61(3):844–879
2. Santos LV et al (2006) Surf Coat Technol 200(8):2587–2593
3. Geetha M et al (2009) Prog Mater Sci 54(3):397–425
4. Murr L et al (2009) J Mech Behav Biomed Mater 2(1):20–32
5. Abdulhadi H et al (2019) J Mater Des Appl 2219–2233
6. Cansizoglu O et al (2008) Mater Sci Eng A 492(1):468–474
7. Feng Q et al (2018) Int J Adv Manuf Technol 94(5):2301–2313
8. Kováčik J et al (1999) J Mater Sci Lett 18(13):1007–1010
9. Francesco T et al (2018) J Comput Inf Sci Eng 18
10. Kobryn PA et al (2001) JOM 53(9):40–42
11. Miao Z et al (2018) Materials 11(12)
12. Zhao M et al (2020) Int J Mech Sci 167:105262
13. Zhang X et al (2018) JOM 75–99
14. Mazur M et al (2017) Laser additive manufacturing. In: Brandt M (ed) Woodhead Publishing, pp 119–161
15. Mazur M et al (2016) Int J Adv Manuf Technol 84(5)
16. Cansizoglu O et al (2006) 17th solid freeform fabrication symposium
17. Alghamdi A et al (2019) Int J Adv Manuf Technol 105(5)
18. Bai L et al (2018) Materials (Basel, Switzerland) 11(10)
19. Epasto G et al (2019) Mater Sci Eng A 753:31–41
20. Maconachie T et al (2019) Mater Des 183:108137
21. T. G. C. TLS (2021) https://www.tls-technik.de
22. ASTM F2924-14 (2021) Book of standards, vol 10.04
23. Baghi A et al (2021) J Manuf Process 68:1031–1046
24. ASM International Handbook (2022) ASM handbook, vol 23A
25. Yilbas BS et al (2019) Heliyon 5(2)
26. Alghamdi A et al (2019) Int J Adv Manuf Technol 105(1)
27. Su X et al (2012) J Mater Process Technol 212(10):2074–2079
28. Wang D et al (2013) Int J Adv Manuf Technol 65(9–12)
29. Agius D et al (2017) Mater Sci Eng, A 701:85–100
30. Gong H et al (2014) Addit Manuf 1–4:87–98
31. Vilaro T et al (2011) Metall Mater Trans A 42(10):3190–3199

32. Kasperovich G et al (2016) Mater Des 105:160–170
33. Baghi A et al (2022) Metals 12(9):1462
34. Yang L et al (2020) J Mater Process Technol 275:116367
35. ASM International Handbook (1989) ASM handbook, vol 16